Numerical Simulation of Free Surface Flows in Die Casting Injection Processes

P. Gómez[1], J. Hernández[1], J. López[2] and F. Faura[2]

[1]Dept. de Mecánica, ETS de Ingenieros Industriales, UNED
Ciudad Universitaria, E-28040 Madrid, Spain
[2]Dept. de Ingeniería de Materiales y Fabricación, ETS de Ingenieros Industriales, UPCT
Pº Alfonso XIII, 48, E-30203 Cartagena, Spain

Abstract

This paper presents a numerical study of the flow of molten metal in the shot sleeve of horizontal high-pressure die-casting machines during the injection process. The analysis of the wave of molten metal created by plunger motion can be of help in reducing porosity in manufactured parts caused by entrapment in the molten metal of a certain amount of the initial air in the die cavity and in the shot sleeve. The amount of trapped air can be reduced by selecting appropriate operating conditions during the injection process, which are mainly determined by the law of plunger motion, the initial shot sleeve filling fraction, and the geometrical characteristics of the shot sleeve. The proposed model, which considers the problem as two-dimensional, is based on the conservation equations of mass and momentum, and treats the free surface using a capturing method (Scalar Equation Method). Surface tension and solidification effects are neglected. Different approaches are considered to simulate plunger motion, in which either the plunger surface or the end wall of the sleeve moves and contracts a Cartesian grid. In the second case, a horizontal body force per unit mass is introduced and the plunger is assumed to be at rest. When numerical results for the wave profile were compared with those obtained using an analytical model based on the shallow-water approximation, and also with numerical results obtained from a CFD code specifically designed for free-surface flow modeling, a good degree of agreement was found.

The calculations were carried out using PHOENICS Version 3.1 on a HP C240 under HP-UX 10.20.

Contents

Introduction

In many die casting injection processes, molten metal is injected into a die cavity from a horizontal shot sleeve in which the metal is pushed by a plunger (Figure 1). The sleeve is partially filled with a volume of molten metal and the plunger then moves the length of the sleeve. In the injection process, a certain amount of the initial air contained in the mold and in the shot sleeve may be trapped in the molten metal and cause porosity when the metal solidifies. The injection process is usually divided into two stages: a stage during which the plunger moves slowly in order to reduce the amount of trapped air, and a fast stage that begins when the shot sleeve is completely filled with molten metal. This work focuses on the slow stage, in which the plunger first forces the molten metal to rise and fill the upper (initially empty) part of the shot sleeve, and then moves at constant speed until the shot sleeve is completely filled with molten metal (Figure 1). The plunger speed needed to raise the wave to the ceiling of the shot sleeve can be easily determined (Tszeng and Chu, 1994; López et al., 2000b). To reach this critical speed, the plunger must be accelerated, and the evolution of the wave profile will obviously depend on the plunger acceleration law employed. Although there are some theoretical (Thome and Brevick, 1993; Brevick et al., 1994; Tszeng and Chu, 1994) and experimental (Karni, 1991; Duran et al., 1991) studies concerning the influence of plunger acceleration on the injection process, in practice relatively little attention has been paid in planning die casting processes to controlling the acceleration of the plunger as it moves to reach its critical speed. An injection system that controls the plunger acceleration at different plunger positions is described by Koch (1974).

Analysis of the free-surface profile evolution for different plunger acceleration law parameters can be of help in determining the operating conditions that minimize the volume of trapped air. Some analytical (López, 2000; López et al., 2000b) and numerical simulations of the flow in the shot sleeve of injection die casting machines (Kuo and Hwang, 1998; Hernández et al., 1999; López, 2000; López et al., 2000a) have been published recently. The objective of this paper is to describe a model of the flow in the shot sleeve implemented

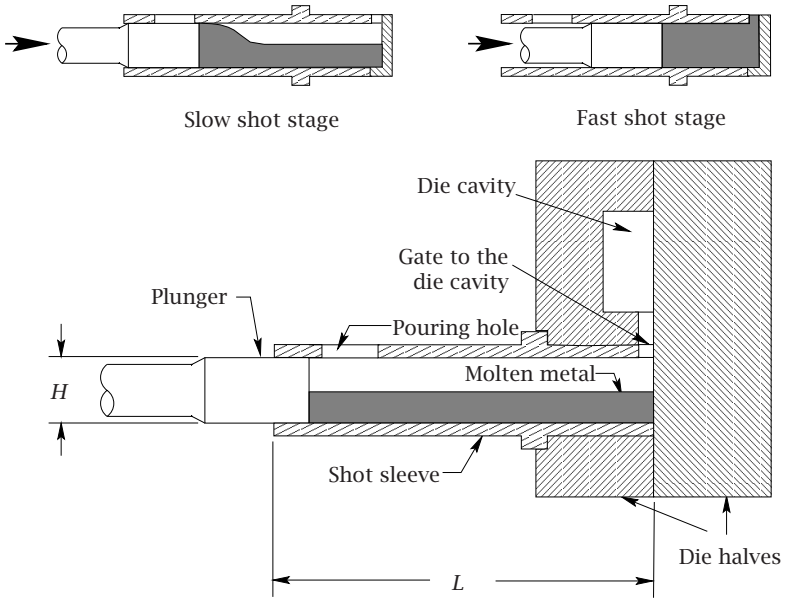

Figure 1: Schematic representation of a die casting machine with horizontal cold chamber.

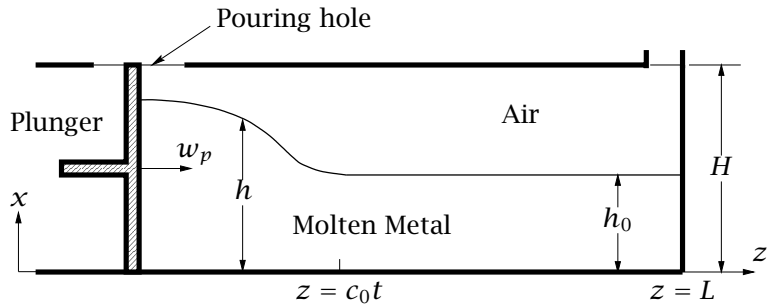

Figure 2: Schematic representation of the problem and coordinate system.

in the PHOENICS code, and to assess its capability in obtaining accurate predictions for the shape of the free surface of molten metal in the shot sleeve. Hernández et al. (1999) presented some preliminary numerical results obtained with this model assuming that the plunger is at rest and reproducing the plunger motion effects by considering a horizontal body force per unit mass acting on the molten metal and imposing the appropriate equivalent boundary conditions. The aim of that preliminary approach, which obviously did not allow the effects of wave reflection against the end wall of the sleeve to be reproduced, was to validate a simplified analytical model based on the shallow-water approximation (López et al., 2000b). In the present work, we basically use the same model employed by Hernández et al. (1999), based on the conservation equations of mass and momentum and the scalar equation method, but we reproduce the relative motion between plunger and the end wall of the sleeve using a Cartesian grid, which is contracted by moving either the plunger surface or the end wall. In the last case, a horizontal body force per unit mass is introduced and the plunger is assumed to be at rest. Numerical results for the wave profile evolution are compared with those obtained using a model based on the shallow-water approximation, which takes into account effects of wave reflection against the end wall of the sleeve (López et al., 2000a), and also with numerical results (Hernández et al., 1999; López et al., 2000a) obtained from a CFD code that was principally developed for free-surface flow modeling (Sant and Backer, 1995).

Governing equations and boundary conditions

Figure 2 shows a schematic representation of the problem and the coordinate system. The problem will be considered as two-dimensional. A single phase treatment has been used for computing the flow of both fluids, molten metal and air. The following governing equations for an incompressible transient flow of a Newtonian fluid will be considered:

$$\frac{\partial u}{\partial x} + \frac{\partial w}{\partial z} = 0, \tag{1}$$

$$\rho\left(\frac{\partial u}{\partial t} + \frac{\partial u^2}{\partial x} + \frac{\partial uw}{\partial z}\right) = -\frac{\partial p}{\partial x} + \mu\left(\frac{\partial^2 u}{\partial x^2} + \frac{\partial^2 u}{\partial z^2}\right) - g\rho, \tag{2}$$

$$\rho\left(\frac{\partial w}{\partial t} + \frac{\partial uw}{\partial x} + \frac{\partial w^2}{\partial z}\right) = -\frac{\partial p}{\partial z} + \mu\left(\frac{\partial^2 w}{\partial x^2} + \frac{\partial^2 w}{\partial z^2}\right) - a_p\rho, \tag{3}$$

where u and w are the velocity components in the Cartesian coordinates x and z, p is the pressure, ρ and μ are the fluid density and viscosity, respectively, and g is the gravitational acceleration. The origins of x and z are at the shot-sleeve floor and the initial plunger face position, respectively. a_p stands for a body force per unit mass corresponding to the plunger acceleration, that will be introduced in some cases, as mentioned above. Surface-tension and solidification effects have been neglected.

In addition to equations (1), (2) and (3), a conservation equation for a scalar 'fluid-marker' variable, F, is solved:

$$\frac{\partial F}{\partial t} + \frac{\partial Fu}{\partial x} + \frac{\partial Fw}{\partial z} = 0. \tag{4}$$

Initially, $F = 0$ in cells containing air and $F = 1$ in cells containing liquid. The location of the free surface is obtained from the solution of equation (4), as defined by points at which $F = 0.5$.

The continuity equation is solved in PHOENICS as the basis of the GALA algorithm in terms of volumetric conservation, avoiding the need of evaluating an average density. Nevertheless, density and viscosity, which change with the type of fluid, are required to solve the momentum conservation equations. This makes it necessary to update the fields of these properties at every instant, which are obtained from the distribution of F using (Liu Jun and Spalding, 1988)

$$\begin{aligned} \rho &= \max\left\{\rho_a, \min\left[\rho_m, \rho_a + (\rho_m - \rho_a)\frac{F - F_a}{F_m - F_a}\right]\right\}, \\ \mu &= \max\left\{\mu_a, \min\left[\mu_m, \mu_a + (\mu_m - \mu_a)\frac{F - F_a}{F_m - F_a}\right]\right\}, \end{aligned} \tag{5}$$

where subscripts a and m indicate air and molten metal, respectively, and F_m and F_a are the values above and below which the cell will be regarded as being full of molten metal and air, respectively.

It is well known that the numerical resolution of equation (4) using continuum advection techniques produces high levels of numerical diffusion. The scalar equation method implemented in PHOENICS tries to reduce the numerical diffusion by using the explicit discretization scheme of Van Leer (1977), in which the F_i value of F convected across the cell face between cells I and $I + 1$ is calculated according to the following expressions:

$$\begin{aligned} F_i &= F_I + \left(\frac{\partial F}{\partial x}\right)_I (\Delta x - u_i \Delta t)/2, \quad \text{for } u_i > 0, \\ F_i &= F_{I+1} - \left(\frac{\partial F}{\partial x}\right)_{I+1} (\Delta x + u_i \Delta t)/2, \quad \text{for } u_i < 0, \end{aligned} \tag{6}$$

where Δx is the size of the grid cell, Δt is the time step, and the values of F and $\partial F/\partial x$ at I and $I + 1$ are those corresponding to the start of the time step.

Three different approaches are used to reproduce the plunger movement. In the first one, a fixed computational mesh is employed, and a body force per unit mass acting on the molten metal, equal to the plunger acceleration at every instant, is introduced. Obviously, with this approach we cannot reproduce the flow in the vicinity of the end wall of the sleeve. In a second approach, in addition to the inertial body force, the end wall of the sleeve moves towards the plunger and contracts the grid, so that effects of wave reflection against the end wall of the sleeve can be simulated. Finally, in a third approach, the plunger moves and contracts the grid, and no body force is required.

A non-slip condition is imposed at the shot sleeve walls and the pressure is fixed at the gate to the mold cavity. At the moving walls the fluid is assumed to have a horizontal velocity (in the appropriate direction) given by the following plunger speed law:

$$w_p = \alpha\beta(e^{\alpha t} - 1), \quad t \le t_H, \tag{7}$$

$$w_p = 2[(gH)^{1/2} - (gh_0)^{1/2}], \quad t > t_H, \tag{8}$$

where α and β are positive constants and

$$t_H = \frac{1}{\alpha} \ln \left[\frac{2(\sqrt{gH} - \sqrt{gh_0})}{\alpha\beta} + 1 \right]. \tag{9}$$

When a body force is introduced to simulate plunger motion, assuming that the plunger is at rest, it is not only the end wall of the sleeve that moves at velocity w_p relative to the plunger, but also the ceiling and bottom walls of the shot sleeve.

As mentioned in the introduction, the numerical results obtained with the proposed model will be compared with those yielded by a model based on the shallow-water approximation, which neglects viscous and non-hydrostatic effects and takes into account the effects of wave reflection against the end wall of the sleeve. The governing equations of this shallow-water model were solved numerically using the method of characteristics and a finite-difference grid based on the inverse marching method. The time t_H defined in equation (9) is the time at which the molten metal would reach the sleeve ceiling according to the shallow-water approximation model.

Computational procedure and PHOENICS settings

The PHOENICS settings used to solve the problem are presented in the q1 file of Appendix A.

Remeshing of the domain is carried out by means of a modified GXPIST subroutine that is activated by making $W1AD = ZMOVE$ in the input file q1 and that includes a special grid remeshing procedure, in combination with an additional subroutine that performs a natural cubic spline interpolation of the variable fields between meshes. In both cases when either the plunger or the end wall of the sleeve moves, only the first cell adjacent to the moving wall is deformed. Although remeshing may require expensive and potentially inaccurate interpolations of solutions, in the cases solved the computing time did not substantially increase and the accuracy was checked as explained below. The reason for using the special grid remeshing procedure just described is that, when the ZMOVE subroutine was used to contract all the grid cells at every time step, a horizontal component of momentum higher than expected was convected in the direction of wave propagation (later, we made some modifications in GROUND subroutine that seemed to overcome these difficulties; these will be published elsewhere). This caused the wave of molten metal to propagate too fast and reach the shot sleeve ceiling too late.

Two different convection discretization schemes, hybrid and MUSCL, were used in the momentum equations. Although MUSCL produced grid-independent solutions for grids appreciably coarser than those required by the hybrid scheme, the advantages of using MUSCL for conditions that make the wave roll up were not so evident when computing time and convergence difficulties were also taken into account.

The explicit formulation used in the conservation equation for the scalar variable meant that the size of the time step had to be limited to ensure stability of the numerical procedure.

The choice of the time step followed the Courant condition:

$$\Delta t < \min\{|\Delta x/u|, |\Delta z/w|\}, \tag{10}$$

where Δx and Δz are the sizes of a grid cell in the x and z directions, respectively, and the minimum refers to every cell in the grid.

Discussion of results and conclusions

The results presented in this section correspond to the plunger motion law of equations (7) and (8), $H = 5.08$ cm, $L/H = 9$, $\beta/H = 0.5$, and a relatively low value of the initial shot sleeve filling fraction $f = h_0/H = 0.254$ (we found greater numerical difficulties for low values of the initial shot sleeve filling fraction). The dynamic viscosity and density of pure aluminum at its freezing point (1.3×10^{-3} Pa s and 2 385 kg m^{-3}, respectively) were used in all computations.

Figure 3 shows a comparison between the numerical results for the wave surface profiles at various instants obtained with PHOENICS and those predicted with the model based on the shallow-water approximation, for three different values of the acceleration parameter α: 1.8, 2.1 and 2.4 (in what follows, instead of α, the dimensionless parameter $\xi = 2c_0/(3\alpha\beta)$, which is the inverse of a Froude number appearing in the analytical study presented by López et al. (2000b), will be used). The shallow-water model predicts that, for $\xi = 4.45$ ($\alpha = 2.1$) and $\xi = 3.89$ ($\alpha = 2.4$), the wave would begin to break (i.e., the wave surface height would become a multi-valued function of z) at $t/t_f = 0.9564$ and $t/t_f = 0.8933$, respectively, so that the model is no longer valid after those instants. The corresponding wave profiles have therefore not been depicted in Figure 3. Also in accordance with the shallow-water model, for a value of $\xi = 4.804$, which is intermediate between those corresponding to Figures 3a and 3b, the wave reflected from the end wall of the sleeve would begin to break just at the instant at which the molten metal reaches the gate to the die cavity. The numerical results from PHOENICS in Figure 3 have been obtained considering a body force acting on the fluid and using a grid which is contracted by a moving shot-sleeve end wall. The hybrid discretization scheme for the convective terms in momentum equations has been used in all cases. From the results of Figure 3 and from those presented in Hernández et al. (1999), it can be observed that there is good agreement between both types of results at sufficiently large distances from the end wall of the sleeve, although the numerical results predict a slightly delayed wave breaking and smoother wave profiles, which is to be expected because the shallow-water model neglects non-hydrostatic effects. For larger values of the initial filling fraction, for which results are not presented here, the delay is more pronounced. In the vicinity of the end wall, wave reflection accentuates the differences between the results of the two models, particularly in regard to the instant at which the molten metal reaches the gate to the die cavity for large values of ξ, which is delayed in numerical results (López et al., 2000a).

In Figure 4 we present a comparison between the numerical results obtained for the free surface height at the plunger face as a function of time and those predicted with the model based on the shallow-water approximation, for the case of Figure 3c. It can be observed that the agreement is very good, and that only for values of t/t_H which are close to 1 do very slight differences appear.

Figure 5 shows, for the same values of the dimensionless parameter ξ of Figure 3, a comparison between the same numerical results of Figure 3 for the wave surface profiles obtained with PHOENICS, and those obtained using the finite-element Wrafts code (Sant and Backer, 1995), which was primarily developed for free-surface transient flow analysis. In

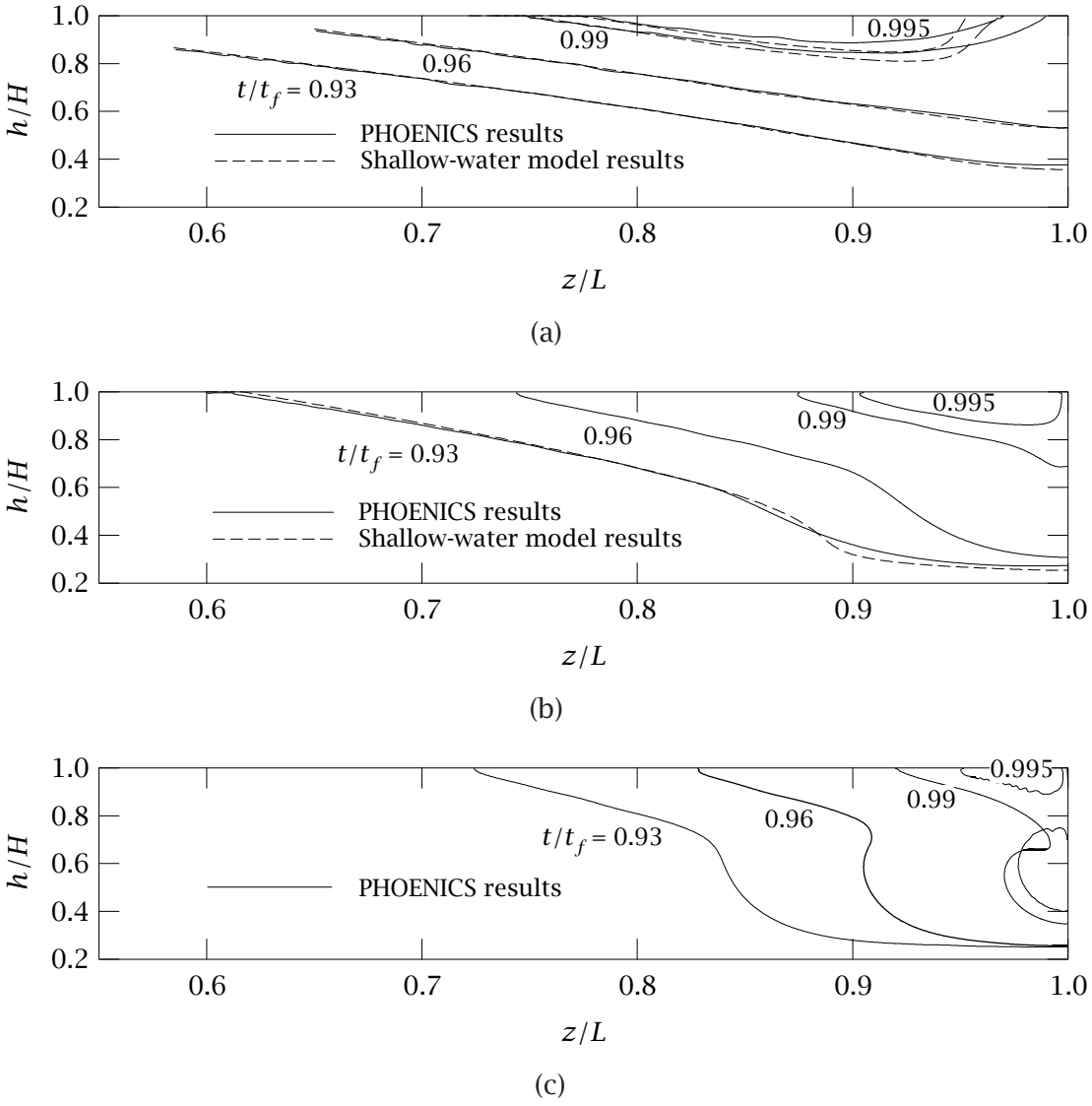

Figure 3: Comparison between results for wave profiles obtained with PHOENICS and those predicted by the shallow-water approximation model. $H = 5.08$ cm, $f = 0.254$, $\beta/H = 0.5$ and $L/H = 9$. a) $\xi = 5.18$; b) $\xi = 4.45$; c) $\xi = 3.89$.

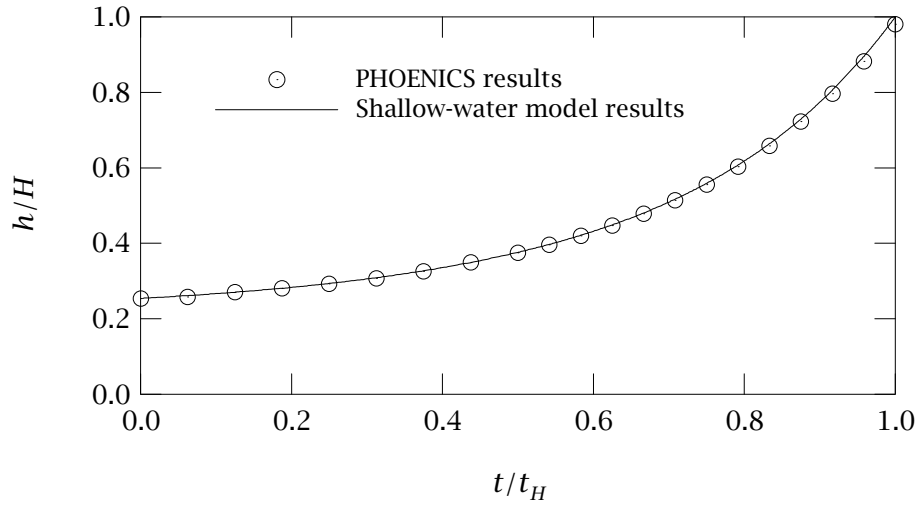

Figure 4: Comparison between numerical and analytical results obtained for the free surface height at the plunger face as a function of time, for the case of Figure 3c.

that code, the momentum equations are solved using an explicit time integration for the velocities, and the pressure is calculated from a Poisson equation at each time step, using the projection method developed by Chorin (1969). The VOF method (Hirt and Nichols, 1981) is used to calculate the position of the free surface, and the mesh is moved and deformed using a technique similar to the Arbitrary Lagrangian-Eulerian method (Hirt et al., 1974). A non-slip condition was imposed at the sleeve walls and the pressure was fixed at the gate to the die cavity. More information on the numerical procedure and details on grid dependence of results can be found in Hernández et al. (1999) and López et al. (2000b). The numerical results from PHOENICS in Figure 3 were obtained considering a body force acting on the fluid and a grid which is contracted by a moving shot-sleeve end wall. It can be observed that the degree of agreement between the results of both codes is good, and that differences are larger in the vicinity of the shot-sleeve end wall. In general, Wrafts results show slightly steeper wave profiles than those obtained with PHOENICS.

Although remeshing increases the difficulty of demonstrating grid independence of the results, different grids were used to check the grid dependence of the solution for the three approaches used to simulate the plunger motion. Except for the wave profiles at the end of the slow stage in working conditions that produce wave rolling (e.g., for t/t_f above a value around 0.95 for $\xi = 3.89$ in Figure 3c), and although a more detailed analysis is probably necessary, nearly grid-independent results were generally obtained when using contracting grids for a grid size of around 160×400 ($NX\times NZ$) elements. Similar conclusions were reached for fixed grids with a higher equivalent initial refinement degree in a zone of the computational domain, of length $L/3.6$, close to the plunger surface (notice that, in this case, the computational domain must extend beyond the end wall of the sleeve; we say that the initial refinement is equivalent when the size of the grid cells near the plunger surface is initially the same in both types of grids). As already mentioned, a grid of size 160×400 was used to obtain the results presented in Figures 3 and 5. Typical time steps varied from 1 ms at the beginning of plunger movement to less than 0.01 ms during wave breaking. Figures 6 and 7 show wave surface profiles at $t/t_f = 0.972$ computed with PHOENICS for the same operating conditions of previous figures and the particular case with $\xi = 3.89$, using different grid sizes, two different discretization schemes for the convective

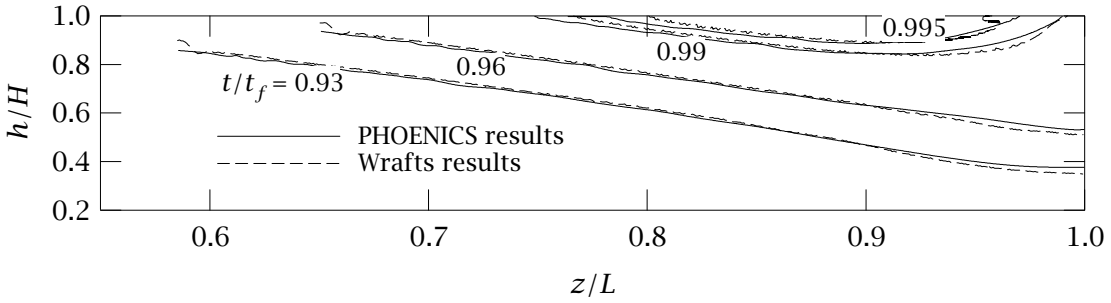

(a)

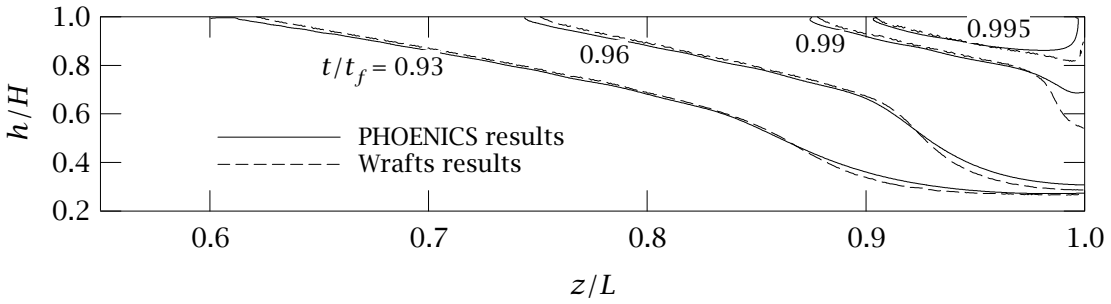

(b)

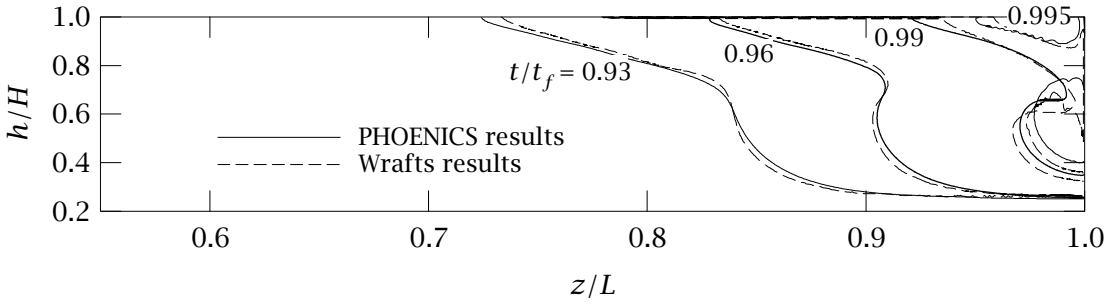

(c)

Figure 5: Comparison between results for wave profiles obtained with PHOENICS and Wrafts codes. $H = 5.08$ cm, $f = 0.254$, $\beta/H = 0.5$ and $L/H = 9$. a) $\xi = 5.18$; b) $\xi = 4.45$; c) $\xi = 3.89$.

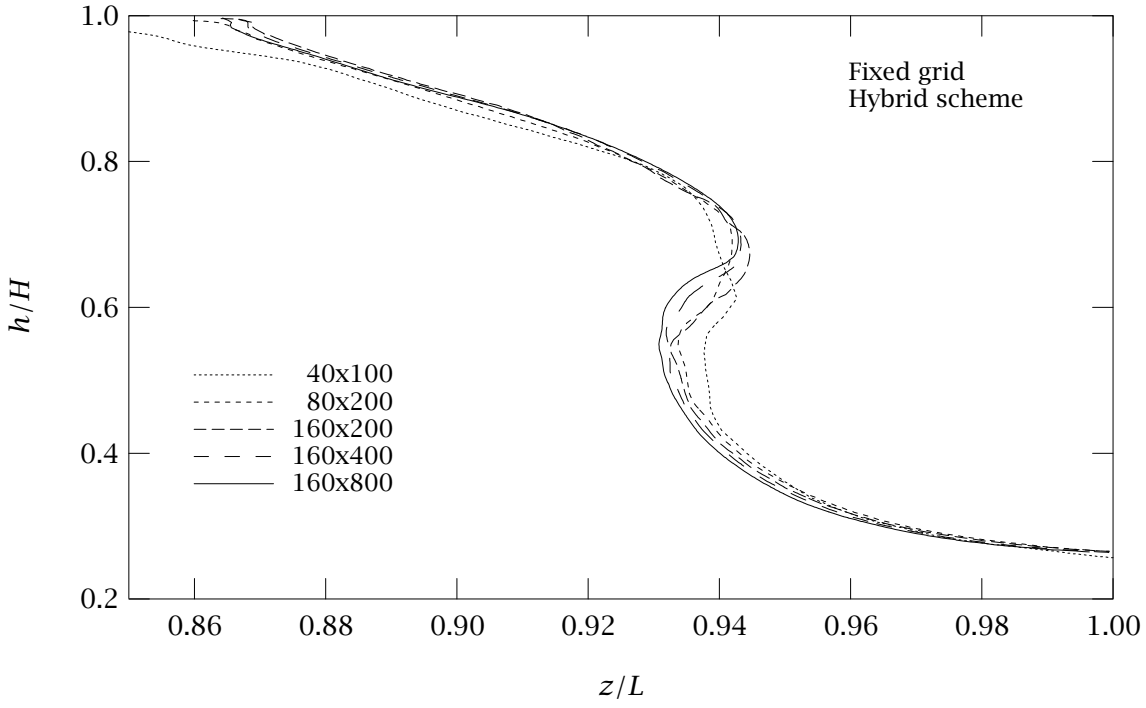

(a)

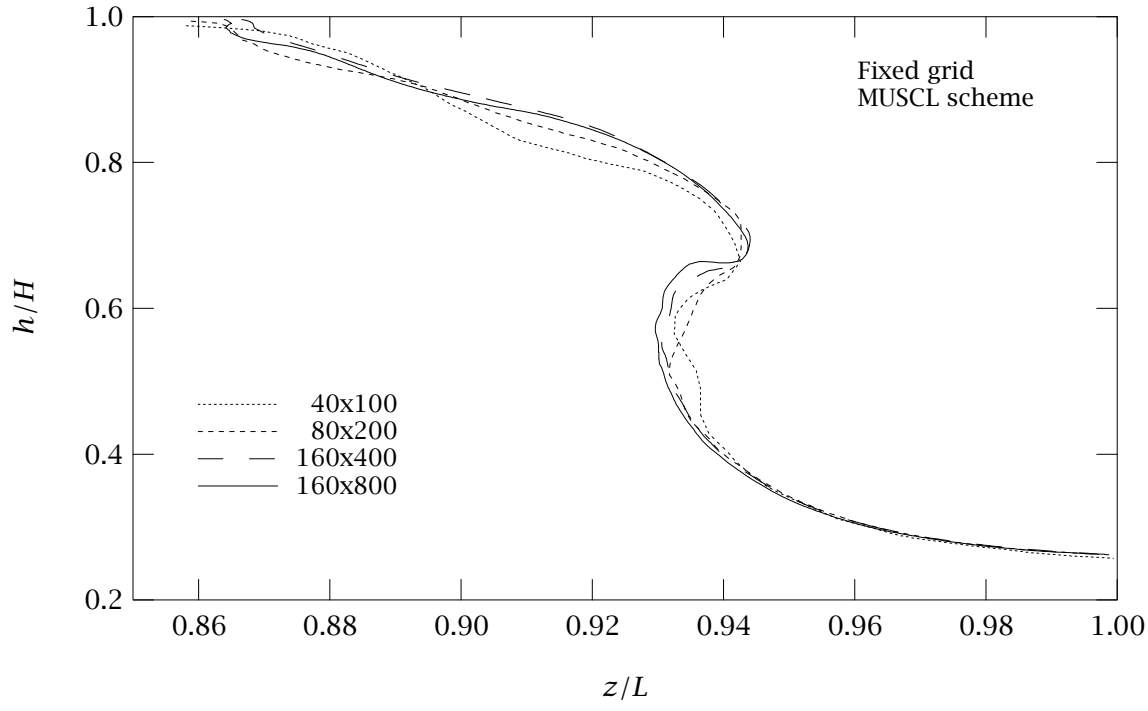

(b)

Figure 6: Wave surface profiles at $t/t_f = 0.972$ computed using a fixed grid. Dependence on grid size and discretization scheme of the convective terms. a) Hybrid scheme. b) MUSCL scheme. ($H = 5.08$ cm, $f = 0.254$, $\xi = 3.89$, $\beta/H = 0.5$ and $L/H = 9$.)

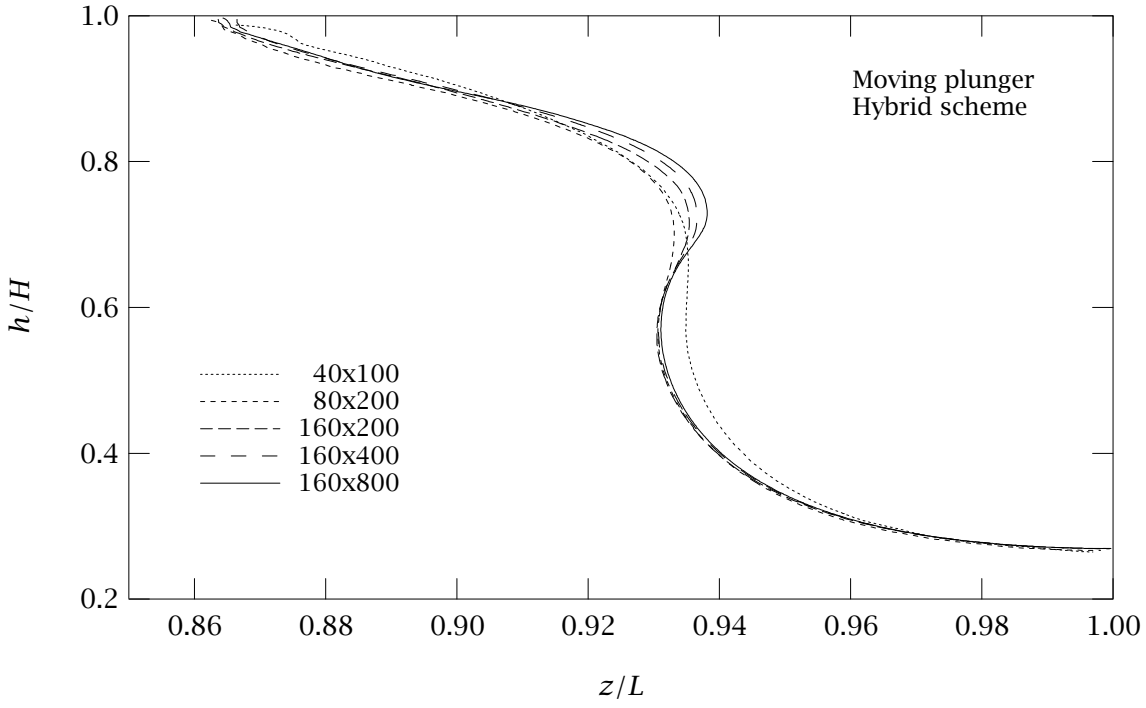

(a)

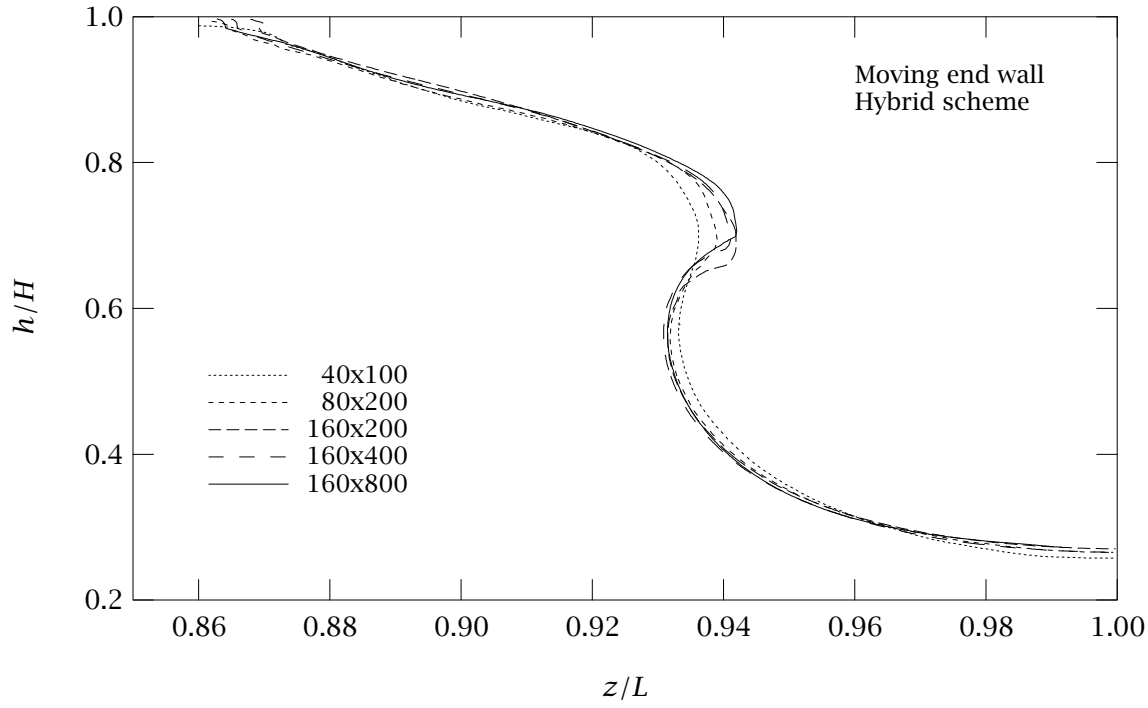

(b)

Figure 7: Dependence on grid size of wave surface profiles at $t/t_f = 0.972$ computed using the hybrid scheme, for two different approaches to simulate plunger motion: a) Moving plunger. b) Inertial body force/moving end wall. ($H = 5.08$ cm, $f = 0.254$, $\xi = 3.89$, $\beta/H = 0.5$ and $L/H = 9$.)

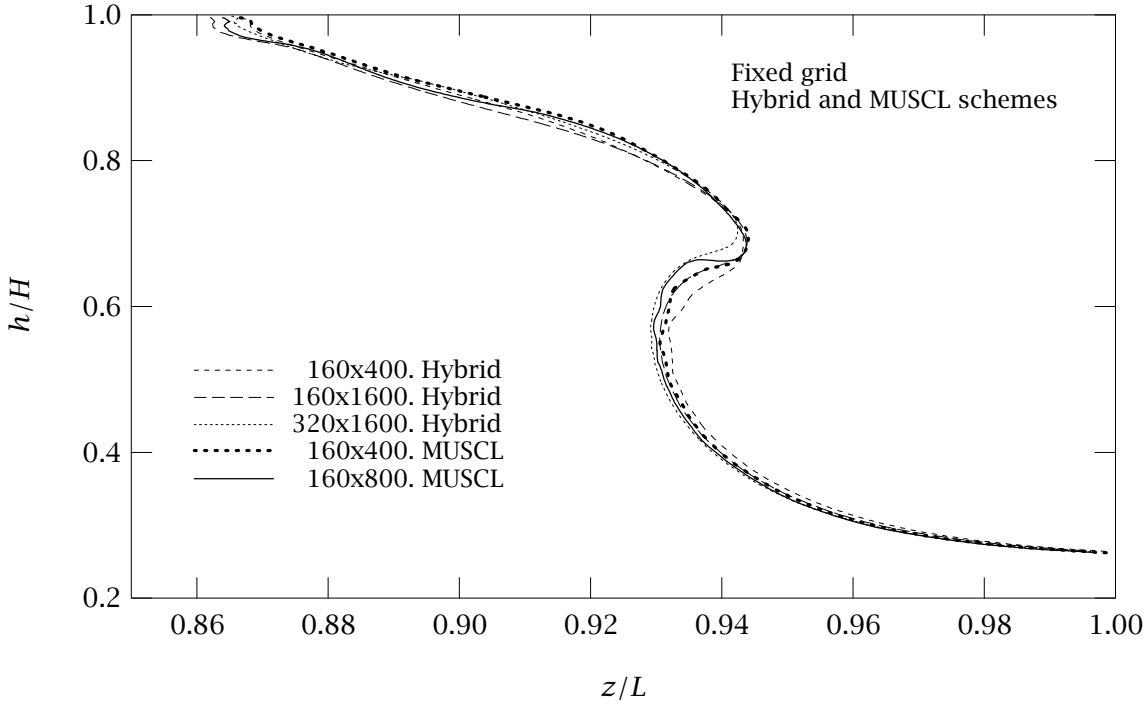

Figure 8: Dependence on grid size of profiles obtained using the MUSCL and Hybrid schemes with a fixed grid. Operating conditions as in Figures 6 and 7 and $t/t_f = 0.972$.

terms in momentum equations, and the three different approaches considered to simulate plunger motion: fixed grid/inertial body force (Figures 6a and 6b); grid contracted by end-wall motion/inertial body force (Figure 7b), and grid contracted by plunger motion (Figure 7a). The hybrid and MUSCL schemes have been used to obtain the results of Figures 6a and 7, and Figure 6b, respectively. The grid sizes indicated in Figure 6 correspond to an equivalent initial refinement degree of a deforming grid as defined above. From these figures, it is clear that grid independence is more difficult to obtain using a grid contracted by the plunger motion. This was the reason for using the alternative approaches based on introducing an inertial body force. Notice that the existence of the shot-sleeve end wall cannot be considered when a fixed grid is used (Figure 6), although in this case the effects of wave reflection against the end-wall still seem to be negligible (at subsequent t/t_f this is not so). The wave profiles obtained introducing a body force and using either a fixed grid or a moving end wall seem to get closer as the grid is refined, although a further and more detailed analysis is required. In the case of a fixed grid, the size of the grid cells at the end of the filling process is obviously larger than that reached when a moving end wall contracts the grid, although this drawback may perhaps be compensated by the advantage that no additional global numerical diffusion is introduced by the remeshing and interpolation procedures required in the case of considering a moving end wall.

Figure 6b shows a comparison between wave profiles obtained using the MUSCL discretization scheme and a fixed grid of different sizes. As expected, this scheme yielded results of a given accuracy for considerably coarser grids, although certain convergence difficulties arose in some cases. In Figure 8 we present numerical results for wave profiles obtained using the MUSCL and Hybrid schemes with a fixed grid of different sizes, which for grid sizes of 160×800 and 320×1600, respectively, can be considered as nearly grid-independent, except possibly around the foremost part of the rolling wave.

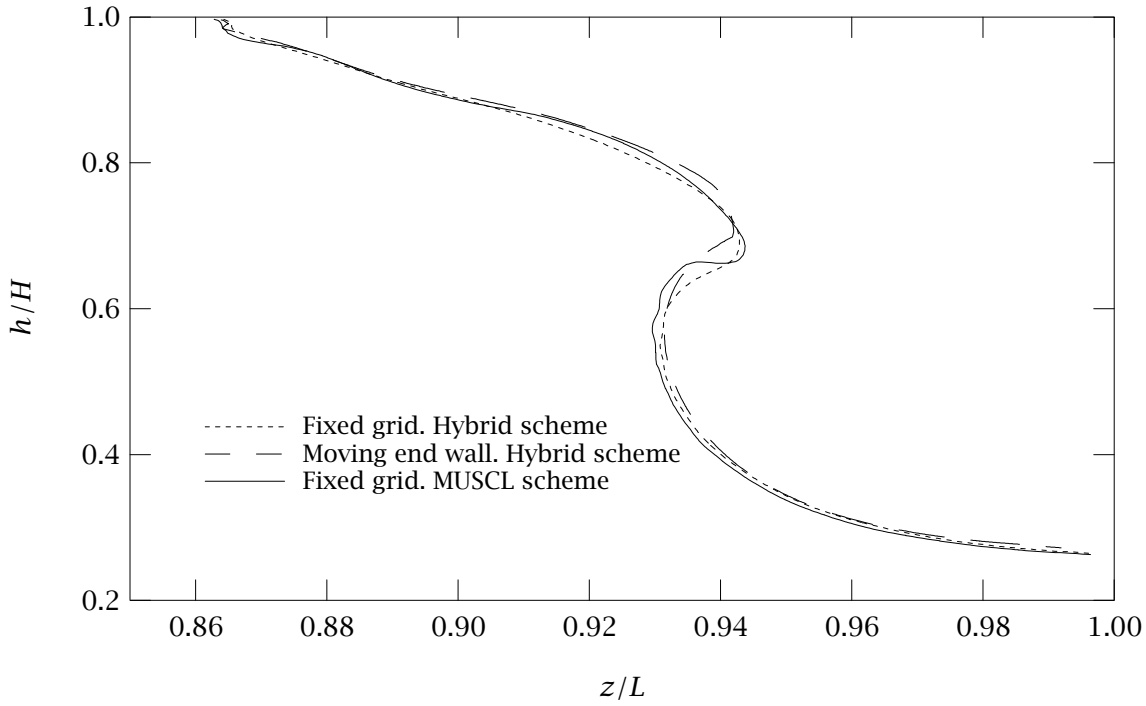

Figure 9: Comparison of profiles obtained using the MUSCL and Hybrid schemes with a fixed grid, and the Hybrid scheme with a moving end wall, with an initially equivalent grid size of 160×800 in the three cases. Operating conditions as in Figures 6 and 7 and $t/t_f = 0.972$.

Figure 9 shows a comparison between wave profiles obtained using the Hybrid discretization scheme, for cases corresponding to both fixed grid and moving end wall calculations, and those obtained using the MUSCL scheme and a fixed grid (the same initially equivalent grid refinement was used in the three cases). Notice that this last profile, which in principle represents a more accurate solution, is intermediate between the first two. This suggests that using a contracting grid in combination with an inertial body force improves the accuracy of the solution obtained using a moving plunger, and allows the effects of wave reflection against the end wall of the sleeve to be reproduced. It should also be pointed out that, although the shot-sleeve operating conditions which the previous discussion on grid dependence refers to are the most severe among those corresponding to the results presented in this work, more cases need to be solved in order to analyze in more detail the grid dependence of results obtained using a moving end wall for broader ranges of operating conditions.

One of the purposes in future works will be to eliminate the unacceptable broadening of the region where the fluid marker variable F varies, which in many operating conditions is unavoidable even when the higher-order monotonic scheme of Van Leer (1977) or other similar techniques are used.

Acknowledgments

The authors gratefully acknowledge the support of the Spanish Comisión Interministerial de Ciencia y Tecnología (CICYT) under grants TAP97-0489 and PB98-0007.

References

Brevick, J. R., Armentrout, D. J., and Chu, Y., 1994, "Minimization of Entrained Gas Porosity in Aluminum Horizontal Cold Chamber Die Casting," *Transactions of NAMRI/SME*, Vol. 22, pp. 41-46.

Chorin, A. J., 1969, "On the Convergence of Discrete Approximations of the Navier-Stokes Equations," *Math. Comput.*, Vol. 23, pp. 341-353.

Duran, M., Karni, Y., Brevick, J., Chu, Y., and Altan, T., 1991, "Minimization of Air Entrapment in the Shot Sleeve of a Die Casting Machine to Reduce Porosity," Technical Report ERC/NSM-C-91-31, The Ohio State University.

Hernández, J., López, J., Gómez, P., and Faura, F., 1999, "Influence of Non-Hydrostatic and Viscous Effects on Shot Sleeve Wave Dynamics in Die Casting Injection," *ASME/JSME Fluids Engineering Conference. Forum on Advances in Free Surface and Interface Fluid Dynamics*, San Francisco, USA, FED-Vol. 248.

Hirt, C. W., Amsden, A. A., and Cook, J. L., 1974, "An Arbitrary Lagrangian-Eulerian Computing Method for all Flow Speeds," *J. Comput. Phys.*, Vol. 14, pp. 227-253.

Hirt, C. W., and Nichols, B. D., 1981, "Volume of Fluid (VOF) Method for the Dynamics of Free Boundaries," *J. Comput. Phys.*, Vol. 39, pp. 201-225.

Karni, Y., 1991, "Selection of Process Variables for Die Casting," Ph.D. thesis, The Ohio State University, Ohio, USA.

Koch, P., 1974, "Parashot System for Turbulence-Free Injection of Metal," *Die Casting Engineer*.

Kuo, T.-H., and Hwang, W.-S., 1998, "Flow Pattern Simulation in Shot Sleeve During Injection of Diecasting," *AFS Transactions*, Vol. 106, pp. 497-503.

Liu Jun and Spalding, D. B., 1988, "Numerical Simulation of Flows with Moving Interfaces," *PhysicoChemical Hydrodynamics*, Vol. 10, No. 5/6, pp. 625-637.

López, J., 2000, "Estudio Analítico y Numérico de los Procesos de Fundición por Inyección a Presión," Ph.D. Thesis, Universidad Politécnica de Cartagena, Spain.

López, J., Hernández, J., Faura, F., and Gómez, P., 2000a, "Effects of Shot Sleeve Wave Reflection on Air Entrapment in Pressure Die Casting Processes," ASME *Fluids Engineering Conference. Symposium on Fluids in Manufacturing Processes*, Boston, USA. Accepted.

López, J., Hernández, J., Faura, F., and Trapaga, G., 2000b, "Shot Sleeve Wave Dynamics in the Slow Phase of Die Casting Injection," ASME *Journal of Fluids Engineering*. Accepted.

Sant, F., and Backer, G., 1995, "Application of WRAFTS Fluid Flow Modeling Software to the Bench Mark Test Casting," *Modeling of Casting, Welding and Advanced Solidification Processes VII*, ed. M. Cross and J. Campbell. Warrendale, PA: TMS, pp. 983-990.

Thome, M. C., and Brevick, J. R., 1993, "Modeling Fluid Flow in Horizontal Cold Chamber Die Casting Shot Sleeves," *AFS Transactions*, Vol. 101, pp. 343-348.

Tszeng, T. C., and Chu, Y. L., 1994, "A Study of Wave Formation in Shot Sleeve of a Die Casting Machine," ASME *Journal of Engineering for Industry*, Vol. 116, No. 2, pp. 175-182.

Van Leer, B., 1977, "Towards the Ultimate Conservative Difference Scheme IV. A New Approach to Numerical Convection," *J. Comput. Phys.*, Vol. 23, pp. 276-299.

Nomenclature

a_p	Plunger acceleration.
c_0	Wave speed relative to the fluid for a depth h_0, $(gh_0)^{1/2}$.
f	Initial shot sleeve filling fraction, h_0/H.
F	Fluid-marker conserved scalar.
g	Gravitational acceleration.
h	Height of the free surface.
h_0	Initial depth of molten metal.
H	Height of the shot sleeve.
L	Length of the shot sleeve.
p	Pressure.
t	Time from start of plunger motion.
t_f	Filling time of the shot sleeve.
t_H	Time at which the molten metal reaches the sleeve ceiling, according to the shallow water model.
u, w	Velocity components.
w_p	Plunger speed.
x, z	Coordinates (Figure 2).
α, β	Parameters in the exponential velocity law of equation (7).
μ	Dynamic viscosity.
ρ	Density.
ξ	Dimensionless parameter, $2c_0/(3\alpha\beta)$.

Subscripts

a	Air.
m	Molten metal.

Appendix A. The q1 file

```
TALK=f;RUN( 1, 1)
    GROUP 1. Run title and other preliminaries
text(Flow in the shot sleeve of high pressure die casting machines)
real(zlast,zlast1,zlast2,timh,timi)
real(xlast,xlast1,xlast2,f,alpha,beta)
integer(nz1,nz2)
integer(nx1,nx2,nnn)
boolean(continuar,zoom,impacto,remesh,inercia,zmove2)
integer(esquema)
  ** MALLA grosera  ** STEADY=F;nx1=10;nx2=30;NY=1;nz1=50;NZ2=50;nnn=1
  ** MALLA FINA     ** STEADY=F;nx1=20;nx2=60;NY=1;nz1=100;NZ2=100;nnn=2
  ** MALLA MUY FINA ** STEADY=F;nx1=30;nx2=90;NY=1;nz1=150;NZ2=150;nnn=3
  ** REFINA         ** STEADY=F;nx1=40;nx2=120;NY=1;nz1=200;NZ2=200;nnn=4
STEADY=F;nx1=10;nx2=30;NY=1; nz1=50;NZ2=50;nnn=1
STEADY=F;nx1=20;nx2=60;NY=1;nz1=100;NZ2=100;nnn=2
STEADY=F;nx1=40;nx2=120;NY=1; nz1=200;NZ2=200;nnn=4
```

```
STEADY=F;nx1=40;nx2=120;NY=1; nz1=200;NZ2=200;nnn=8
  tfirst=1.204
alpha=2.4
beta =0.0254
zmove2=f
impacto=t
remesh=t
inercia=t
zoom=f
f=0.254
timh=1.052
timi=1.18
xlast=.0508;zlast=.4572
zlast1=zlast/2.
zlast2=zlast/2.
xlast1=xlast*f
xlast2=xlast*(1.-f)
    GROUP 2. Transience; time-step specification
NREGT=2
IREGT=1;GRDPWR(T,10*nnn,.1213917*2,1.0)
IREGT=2;GRDPWR(T,30*nnn,.1213917*2,1.0)
IREGT=3;GRDPWR(T,30*nnn,.1213917*1,1.0)
IREGT=4;GRDPWR(T,40*nnn,.1213917*1,1.0)
IREGT=5;GRDPWR(T,60*nnn,.1213917,1.0)
IREGT=6;GRDPWR(T,100*nnn,.1213917,1.0)
IREGT=7;GRDPWR(T,180*nnn,.1213917,1.0)
IREGT=8;GRDPWR(T,60*nnn,.1213917*.3,1.0)
IREGT=9;GRDPWR(T,180*nnn,.1213917*.6,1.0)
IREGT=10;GRDPWR(T,100*nnn,.1213917*.1,1.0)
    GROUP 3. X-direction grid specification
NREGX=2
IREGX=1;GRDPWR(X,Nx1,xlast1,1.0)
IREGX=2;GRDPWR(X,Nx2,xlast2,1.0)
    GROUP 5. Z-direction grid specification
NREGZ=2
IREGZ=1;GRDPWR(Z,nz1,zlast1,1.0)
IREGZ=2;GRDPWR(Z,nz2,zlast2,1.0)
    GROUP 6. Body-fitted coordinates or grid distortion
    GROUP 7. Variables stored, solved & named
SOLUTN(P1,Y,Y,Y,P,P,P); OUTPUT(P1,Y,Y,Y,Y,Y,Y)
SOLUTN(U1,Y,Y,Y,P,P,P); OUTPUT(U1,Y,Y,Y,Y,Y,Y)
SOLUTN(W1,Y,Y,Y,P,P,P); OUTPUT(W1,Y,Y,Y,Y,Y,Y)
esquema=1
  scheme(smart,u1,w1);esquema=3
  scheme(muscl,u1,w1);esquema=3
STORE(RHO1,PRPS); SOLVE(VFOL,SURN); STORE(ENUL)
    GROUP 8. Terms (in differential equations) & devices
GALA=T; TERMS(VFOL,N,N,N,N,P,P);TERMS(SURN,N,N,N,N,P,P)
    GROUP 9. Properties of the medium (or media)
RHO1=GRND10;ENUL=GRND10
    GROUP 11. Initialization of variable or porosity fields
FIINIT(P1)=0.0;FIINIT(U1)=0.0;FIINIT(V1)=0.0;FIINIT(W1)=1e-10
FIINIT(PRPS)=0;FIINIT(SURN)=0.0;FIINIT(rho1)=1.189;INIADD=F
    GROUP 13. Boundary conditions and special sources
PATCH(WATER,INIVAL,1,nx1,1,ny,1,nz,1,1)
COVAL(WATER,VFOL,0,1)
```

```
COVAL(WATER,SURN,0,1)
COVAL(WATER,PRPs,0,67)
restrt(all);continuar=t
integer(nzsal,nzsal2)
nzsal=nz*9/10-2*nnn
nzsal2=nz*1/10+2*nnn
if(inercia) then
PATCH(SALI,east,nx,NX,1,1,nzsal,nz,1,LSTEP)
else
PATCH(SALI,east,nx,NX,1,1,1,nzsal2,1,LSTEP)
endif
COVAL(SALI,p1,1.0,0.0)
COVAL(SALI,surn,fixflu,grnd1)
PATCH(TCON,CELL,1,NX,1,NY,1,NZ,1,LSTEP)
COVAL(TCON,SURN,GRND,GRND)
WALL(wall1,low,1,nx,1,ny,1,1,1,lstep)
WALL(wall3,high,1,nx,1,ny,nz,nz,1,lstep)
if(inercia) then
wall(wall2,east,nx,nx,1,ny,1,nzsal-1,1,lstep)
value(wall2,w1,grnd)
else
if(zmove2.eq.false) then
wall(wall2,east,nx,nx,1,ny,nzsal2+1,nz,1,lstep)
value(wall2,w1,0.0)
endif
endif
  Gravity-force source of V1
PATCH(GRAV,PHASEM,1,NX,1,NY,1,NZ,1,LSTEP)
COVAL(GRAV,u1,FIXFLU,-9.81)
if (inercia) then
COVAL(GRAV,w1,FIXFLU,grnd)
endif
    GROUP 15. Termination of sweeps
LSWEEP=12
    GROUP 16. Termination of iterations
LITER(SURN)=1
    GROUP 17. Under-relaxation devices
real(dtf); dtf=1.
if(scheme.gt.1) then
RELAX(V1,FALSDT,dtf);RELAX(W1,FALSDT,dtf)
endif
USEGRX=T;USEGRD=t
    GROUP 19. Data communicated by satellite to GROUND
w1ad=ZMOVE; AZW1=alpha ; BZW1=beta; CZW1=4.0; IZW1=nz-1
real(dist1,dist2,dist3,dist4)
real( ZWO1,ZWO2,ZWO3,ZWN1,ZWN2,ZWN3)
integer(IZW2,IZW3)
izw2=nz;izw3=nz
if (impacto) then
izw1=nz;izw2=nz;izw3=nz
endif
SPEDAT(PISTO, timh, R,timh)
SPEDAT(PISTO, timi, R,timi)
SPEDAT(PISTO, continuar, L,continuar)
SPEDAT(PISTO, impacto, L,impacto)
SPEDAT(PISTO, zoom, L,zoom)
```

```
SPEDAT(PISTO, remesh, L,remesh)
SPEDAT(PISTO, dist4, R, 1.e-7)
SPEDAT(PISTO, inercia, L,inercia)
SPEDAT(PISTO, esquema, I,esquema)
SPEDAT(PISTO, zmove2, L,zmove2)
if(.not.continuar) then
SPEDAT(PISTO, IZW1, I, :izw1:)
SPEDAT(PISTO, IZW2, I, izw2)
SPEDAT(PISTO, IZW3, I, izw3)
SPEDAT(PISTO, dist3, R, 0.0)
else
dist1  = 0.0; dist2  = 1.945E-05; dist3  =  .000E+00
izw1=400;izw2=400;izw3=400
SPEDAT(PISTO, IZW1, I, izw1)
SPEDAT(PISTO, IZW2, I, IZW2)
SPEDAT(PISTO, IZW3, I, IZW3)
SPEDAT(PISTO, dist1, R,dist1)
SPEDAT(PISTO, dist3, R,dist3)
SPEDAT(PISTO, zwo(1), R, ZWO1)
SPEDAT(PISTO, zwo(3), R, ZWO3)
endif
IPRPSA=67;IPRPSB=0
IDISPA=30*nnn
IHOLA=1
SURF=T;RLOLIM=0.49;RUPLIM=0.51
csg1=c;csg2=XYZ
VARMIN(SURN)=0.0; VARMAX(SURN)=1.0
tstswp=-1;ixmon=nx1;iymon=1;izmon=nz-1
    GROUP 23. Field print-out and plot control
NPLT=1
NTPRIN=LSTEP/100;OUTPUT(P1,Y,Y,Y,Y,Y,Y);OUTPUT(V1,Y,Y,Y,Y,Y,Y)
OUTPUT(W1,Y,Y,Y,Y,Y,Y);OUTPUT(vfol,Y,N,y,N,N,N)
OUTPUT(DEN1,Y,N,y,N,N,N)
IPLTF=20;XZPR=T;itabl=1
if(:czw1:.eq.4) then
mesg(
mesg( ############################################################
mesg( #             CONTRACCION GRADUAL                          #
mesg( ############################################################
mesg(
endif
mesg(
mesg( ############################################################
mesg( #  alpha=:azw1:, beta=:bzw1:, f=:f:       #
mesg( ############################################################
mesg(
if(:tfirst:.ne.0.and.continuar) then
mesg(
mesg( ############################################################
mesg( #             continua en :tfirst:                         #
mesg( ############################################################
mesg(
mesg(
endif
STOP
```